Available *online* at : http://jnte.ft.unand.ac.id/

Jurnal Nasional Teknik Elektro

| ISSN (Print) 2302-2949 | ISSN (Online) 2407-7267 |

Effect of MXene Loading on the Structure and Electrochemical Performance of Biodegradable PVA/ZnO/MXene/CNC Composite Films

Rudy Fernandez[1,2], *Hairul Abral*[*2], *Ikhwana Elfitri*[1], *Syukri Yunus*[1]

[1] *Departemen Teknik Elektro,Universitas Andalas, Indonesia*
[2] *Departemen Teknik Mesin, Universitas Andalas, Indonesia*

ARTICLE INFORMATION

Received: February 28, 2026
Revised: March 24, 2026
Accepted: March, 26, 2026
Available online: March 29, 2026

KEYWORDS

Biodegradable composite films; MXene ($Ti_3C_2T_x$); Poly(vinyl alcohol); Specific capacitance; Current density; Conductive network; Dispersion–percolation mechanism

CORRESPONDENCE

E-mail: abral@eng.unand.ac.id

A B S T R A C T

The growing demand for sustainable materials for flexible electronics and energy storage applications has driven the development of biodegradable composite films with enhanced electrochemical functionality. This study systematically investigates the effect of MXene loading on the structure, morphology, and electrochemical performance of biodegradable PVA/ZnO/MXene/CNC composite films fabricated by aqueous solution casting. The main contribution of this work is the explicit establishment of a relationship between loading, structure, and electrochemical performance for this multicomponent biodegradable film system under controlled processing conditions. Films containing 20%, 25%, and 30% MXene were prepared with constant ZnO and CNC contents and characterized by X-ray diffraction (XRD), field-emission scanning electron microscopy (FESEM), and cyclic voltammetry in 1 M KOH. The crystallinity increased from 20.06% to 27.58% and 44.74% with increasing MXene loading, while FESEM revealed progressively more homogeneous morphology and improved filler dispersion. These structural changes were accompanied by a marked enhancement in electrochemical response, with current density increasing from 425.18 to 876.71 and 1480.25 A/m², and specific capacitance rising from 0.921966 to 1.682536 and 2.860035 F/g for 20%, 25%, and 30% MXene, respectively. The 30% MXene film exhibited the best overall performance, indicating that higher MXene loading within the investigated range promotes more continuous conductive pathways and greater electroactive surface accessibility. These findings provide useful insight for designing biodegradable composite films for sustainable flexible energy-storage applications.

INTRODUCTION

The rapid growth of portable, wearable, and flexible electronic devices has increased demand for material systems that combine electrochemical functionality with environmental sustainability. Conventional electronic materials are typically based on rigid, non-biodegradable components, creating disposal challenges and contributing to electronic waste. As a result, biodegradable and flexible materials have become increasingly important for next-generation electronics and energy-storage applications [1]. In particular, flexible supercapacitors require materials that provide sufficient conductivity and charge-storage capability while maintaining processability, mechanical adaptability, and environmental compatibility [2]-[6].

Polymer-based composites are attractive in this context because they combine the low density, flexibility, and solution processability of polymers with the functional advantages of conductive or reinforcing fillers [1]-[4]. Among water-processable and biodegradable polymers, poly(vinyl alcohol) (PVA) is widely used because of its excellent film-forming ability, good mechanical integrity, and compatibility with flexible electrochemical systems [2], [5], [7]. However, the inherently insulating nature of PVA limits its direct use in energy-storage applications, making the incorporation of conductive and structurally active fillers essential for improving charge transport and electrochemical response [1], [2], [7], [8].

ZnO and $Ti_3C_2T_x$ MXene are particularly relevant fillers for such composite systems. ZnO has been incorporated into polymer

https://doi.org/10.25077/jnte.v15n1.1555.2026

matrices because of its chemical and thermal stability and its ability to modify the structural and electrical behavior of the host matrix [1], [6]-[9]. MXene, on the other hand, has attracted strong interest as a conductive filler due to its high electrical conductivity, hydrophilic surface terminations, and good compatibility with polar polymers [2], [3], [10]. Previous studies have shown that MXene can improve conductivity and functional performance in flexible composite films and related electrochemical materials [11]-[14]. However, its practical benefit depends strongly on maintaining nanosheet dispersion, as MXene is prone to restacking via van der Waals interactions, thereby reducing accessible surface area and potentially hindering ion and electron transport [15]-[17]. For this reason, the performance of MXene-based composites is governed not only by filler presence, but also by how effectively the conductive network and electrochemically accessible interfaces are preserved during composite formation [16]-[18].

Cellulose nanocrystals (CNCs) offer a bio-derived route to improve this structural stability. Owing to their high crystallinity, stiffness, and large specific surface area, CNCs can serve as reinforcing agents and hydrophilic spacers in polymer composites [19], [20]. In MXene-containing systems, they are expected to reduce sheet restacking, promote filler dispersion, and stabilize the composite structure through hydrogen-bond-mediated interactions [13], [16], [18]. In addition, processing strategy is an important factor in determining final morphology and performance. Sonication-assisted mixing has been widely used to reduce nanofiller agglomeration and improve dispersion homogeneity in solution-processed composites [21]-[24]. At the same time, previous studies indicate that the effect of MXene loading in PVA-based systems may not be strictly linear, because gains in conductive-network formation can eventually be limited by aggregation or interfacial transport constraints when dispersion becomes less effective at higher filler content [13], [14].

Although biodegradable polymers for green electronics [1], [2], PVA-based composite films [5], [8], ZnO/PVA materials [6]-[9], and MXene-based conductive composites [10]-[18], [25]-[27] have all been widely reported, systematic studies on incremental MXene loading in biodegradable PVA/ZnO/MXene/CNC composite films under matched processing and electrochemical conditions remain limited. More specifically, previous studies have not clearly established how variations in MXene loading affect structural ordering, morphology, current density, and specific capacitance within this multicomponent biodegradable film platform.

In response to this gap, this study investigates the effect of MXene loading on the structure and electrochemical performance of biodegradable PVA/ZnO/MXene/CNC composite films through a controlled comparison of three MXene contents (20%, 25%, and 30%), while keeping the matrix system, ZnO and CNC contents, and processing conditions constant. The novelty of this work lies in its direct loading-dependent analysis of structure–performance relationships in a biodegradable multicomponent film system under controlled preparation conditions. X-ray diffraction (XRD) and field-emission scanning electron microscopy (FESEM) were used to evaluate crystallinity and morphology, while cyclic voltammetry was used to determine current density and specific capacitance. By linking MXene content to structural evolution, morphological uniformity, and electrochemical response, this work specifically addresses a limitation of previous studies: the lack of a clear, controlled correlation between MXene loading and electrochemical behavior in biodegradable PVA/ZnO/MXene/CNC composite films for sustainable flexible energy-storage applications**.**

METHODS

Materials and Composition Design

Poly(vinyl alcohol) (PVA) was used as the biodegradable polymer matrix due to its excellent aqueous processability, film-forming ability, and compatibility with flexible electrochemical systems [25]. ZnO was incorporated as an inorganic filler to provide structural and interfacial modification within the polymer matrix, whereas $Ti_3C_2T_x$ MXene was used as the primary conductive phase to promote charge-transport pathways in the composite films [25]-[30]. Cellulose nanocrystals (CNCs) were included as a bio-derived nanofiller to improve structural integrity and enhance filler dispersion, particularly by suppressing MXene restacking through hydrophilic and hydrogen-bond-mediated interactions [13], [18], [25].

To evaluate the effect of MXene loading under identical processing conditions, three composite formulations were prepared by varying only the masses of PVA and MXene, while keeping the amounts of ZnO, CNC, and solvent, as well as the processing parameters, constant. The formulations corresponded to MXene contents of 20%, 25%, and 30%, with PVA/MXene masses of 1.32 g/0.40 g, 1.22 g/0.50 g, and 1.12 g/0.60 g, respectively. In all formulations, the ZnO mass was fixed at 0.16 g and the CNC mass at 0.12 g. Deionized water was used as the solvent, consisting of 20 mL for the PVA/ZnO solution and 20 mL for the CNC/MXene suspension.

Preparation of PVA/ZnO Solution

The PVA/ZnO precursor solution was prepared by dissolving the required amount of PVA in 20 mL deionized water at 80 °C under magnetic stirring at 500 rpm for 30 min until a clear and homogeneous solution was obtained. After complete dissolution, 0.16 g ZnO was added to the PVA solution and the mixture was stirred under the same conditions for another 30 min to promote uniform dispersion. The resulting suspension was then ultrasonicated for 10 min to improve particle distribution before blending with the MXene/CNC suspension.

Preparation of MXene/CNC Solution

Separately, 0.12 g CNC was dispersed in 20 mL deionized water and stirred at 80 °C and 500 rpm for 30 min. MXene was then gradually introduced into the CNC suspension to achieve the target compositions (0.40, 0.50, or 0.60 g for 20%, 25%, and 30% MXene, respectively), while maintaining the same stirring conditions. The suspension was subsequently ultrasonicated for 60 min to improve homogeneity and reduce the likelihood of MXene agglomeration and restacking [25]-[27].

Blending, Film Casting, and Drying

https://doi.org/10.25077/jnte.v15n1.1555.2026

The MXene/CNC suspension was added into the PVA/ZnO solution and the combined mixture was stirred at 80 °C and 500 rpm for 20 min until a visually homogeneous slurry was formed. To minimize material loss and maintain compositional consistency among samples, the MXene/CNC container was rinsed with 5 mL deionized water, and the rinse solution was added to the main slurry. The resulting slurry was cast into a petri dish and dried in an oven at 60 °C for 5 h to obtain solid composite films. After drying, the films were left at room temperature for 5 min, then stored in a desiccator prior to characterization to minimize moisture uptake.

Characterization and Electrochemical Measurements

The structure of the composite films was analyzed by X-ray diffraction (XRD) to evaluate crystallinity and structural ordering as a function of MXene loading. Surface morphology and filler distribution were examined using field-emission scanning electron microscopy (FESEM). Electrochemical performance was evaluated by cyclic voltammetry (CV) in 1 M KOH electrolyte using an Ag/AgCl reference electrode and a Pt counter electrode over the potential window described in the Results and Discussion section. CV measurements were used to determine current density and specific capacitance for comparative analysis of the three MXene-loading films.

Experimental Design Rationale

The experimental procedure was designed to ensure that differences in structure, morphology, and electrochemical performance could be attributed primarily to variation in MXene loading. Therefore, ZnO content, CNC content, solvent volume, stirring conditions, ultrasonication duration, casting procedure, and drying conditions were kept constant for all samples. This controlled design enabled direct evaluation of the relationship between MXene content and the resulting structural and electrochemical properties of the biodegradable PVA/ZnO/MXene/CNC composite films.

RESULTS AND DISCUSSION

Structural Evolution of PVA/ZnO/MXene/CNC Films

Figure 1 presents the X-ray diffraction (XRD) patterns of the PVA/ZnO/MXene/CNC composite films with MXene loadings of 20%, 25%, and 30%, together with their comparative overlay. The diffractograms confirm the semicrystalline character of the composite films, which is consistent with the partial structural ordering of PVA and the contribution of filler-induced organization within the multicomponent matrix. As the MXene content increased, the diffraction intensity became progressively more pronounced, suggesting that higher filler loading promoted greater structural ordering by increasing the contribution of lamellar MXene domains and by influencing matrix organization during film formation. This trend is consistent with previous reports showing that MXene-containing composites can exhibit stronger diffraction features as the fraction of lamellar or partially ordered MXene domains increases [25], [30]. Because MXene nanosheets are susceptible to van der Waals-driven restacking, the increase in diffraction intensity may reflect not only a larger contribution from MXene-derived ordered domains, but also closer interfacial packing among MXene, PVA, and CNC, which could favor the formation of more continuous transport pathways.

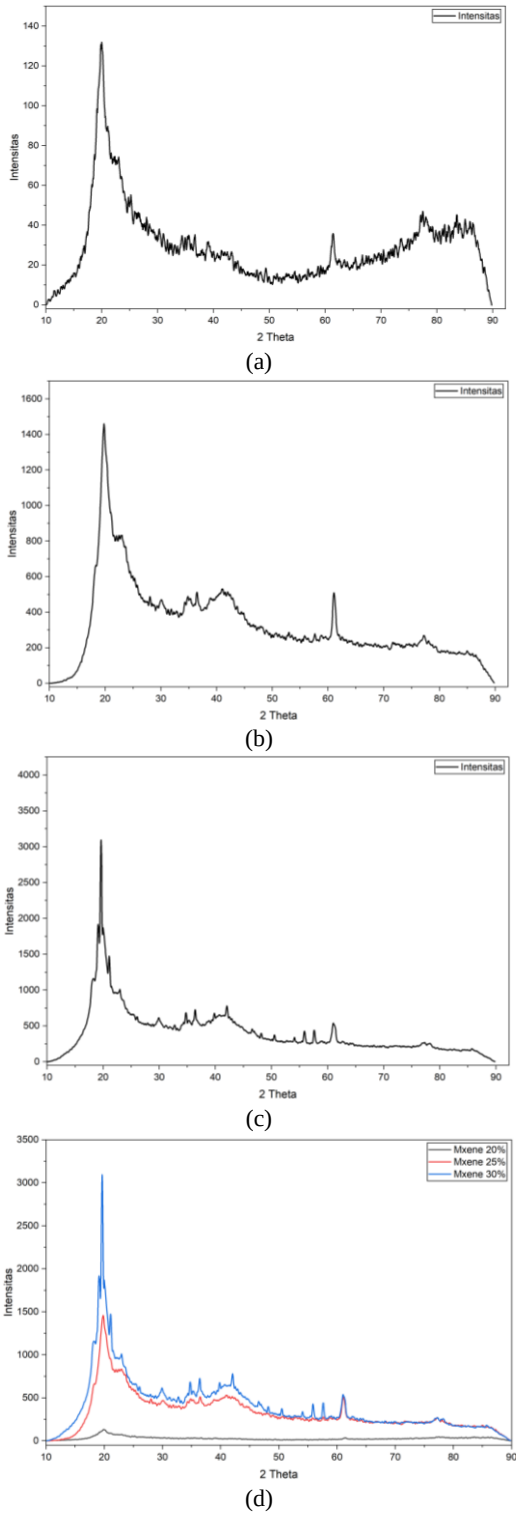

Figure 1. Crystallinity in XRD patterns for (a)20%, (b) 25%, (c) 30% and (d) the comparison of three loadings.

The crystallinity values calculated from the XRD patterns are summarized in Table 1. The crystallinity increased from 20.06% in the 20% MXene film to 27.58% in the 25% film and 44.74% in the 30% film. This monotonic increase suggests that higher MXene loading promoted a more ordered composite structure during film formation, likely by increasing the density of

interfacial sites that influenced chain arrangement and filler organization as the solvent evaporated. Such behavior may be associated with the increasing role of MXene as a heterogeneous nucleation site, together with interfacial interactions among MXene, PVA, and CNC during solvent evaporation and film solidification, which may have facilitated local chain rearrangement and more stable filler–matrix packing [31]. Relative to the 20% film, crystallinity increased by approximately 37.5% in the 25% film and 123.0% in the 30% film, indicating substantial structural reorganization across the investigated loading range.

Table 1. XRD-derived crystallinity of PVA/ZnO/Mxene/CNC films.

MXene content (%)	Crystallinity (%)
20	20.06
25	27.58
30	44.74

Although the increase in crystallinity suggests improved structural organization, this result should not be interpreted solely as evidence of enhanced polymer ordering. In MXene-based composites, higher apparent ordering may also indicate an increased contribution from lamellar MXene domains. Therefore, the structural significance of the XRD results is better understood in relation to the FESEM and electrochemical data discussed below. In the present study, the XRD results provide a key structural basis for understanding how MXene loading influences the formation of conductive pathways and electrochemically active interfaces in the biodegradable composite films.

Morphological Characteristic and Filler Dispersion

The surface morphology of the composite films was analyzed by field-emission scanning electron microscopy (FESEM), as shown in Figures 2–4. The FESEM observations reveal a clear evolution in surface uniformity and filler distribution as the MXene content increased. In MXene–polymer systems, homogeneous morphology, reduced agglomeration, and fewer restacked domains are generally associated with improved conductive-network formation and enhanced electrochemical accessibility [25], [27].

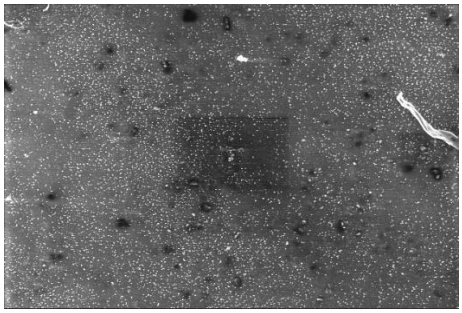

Figure 2. FESEM result for 20% MXene loading

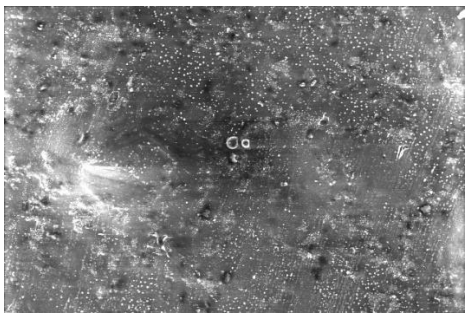

Figure 3. FESEM result for 25% MXene loading.

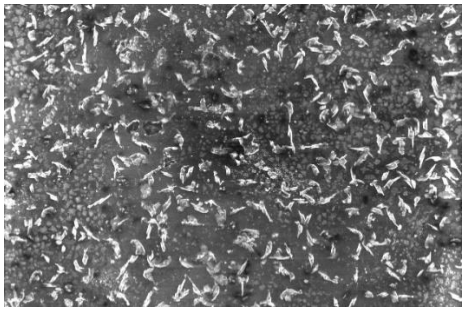

Figure 4. FESEM result for 30% MXene loading.

At 20% MXene (Figure 2), the film surface appears relatively smooth but still shows non-uniform particle distribution and localized agglomeration. This morphology suggests that the conductive filler had not yet been evenly distributed throughout the matrix, resulting in isolated conductive domains and reduced transport continuity. At 25% MXene (Figure 3), the surface becomes more homogeneous, indicating improved dispersion and better integration of MXene within the PVA/ZnO/CNC matrix, likely because the available CNC-assisted spacing and sonication energy were still sufficient to separate the nanosheets and distribute them more evenly throughout the matrix. The 30% MXene film (Figure 4) exhibits the most uniform and densely integrated morphology among the three samples, with broader filler coverage and without dominant large agglomerates, suggesting that the processing conditions were still able to maintain effective sheet separation and interfacial distribution even at the highest loading examined. This observation suggests that the selected processing route maintained satisfactory dispersion even at the highest MXene loading investigated, likely because sequential mixing and prolonged ultrasonication reduced local agglomeration and improved MXene distribution in the CNC-containing suspension prior to film casting.

The progressive morphological improvement from 20% to 30% MXene is consistent with the controlled solution-processing approach used in this study, particularly the sequential mixing and prolonged ultrasonication of the MXene/CNC suspension. Related studies have likewise reported that MXene/cellulose-based composites and degradable MXene-containing systems benefit from interfacial interactions that help reduce sheet collapse, improve spacing, and promote structural continuity [16], [18], [25]. Therefore, the FESEM results support the interpretation that increasing MXene loading, when combined with CNC-assisted dispersion and controlled processing, facilitates the development of a more continuous conductive

https://doi.org/10.25077/jnte.v15n1.1555.2026

network by reducing interparticle separation and increasing the probability of filler-to-filler contact across the composite films.

Electrochemical Response and Current Density Enhancement

The electrochemical behavior of the composite films was evaluated by cyclic voltammetry (CV) in 1 M KOH over the potential range of −0.2 V to +0.6 V, using an Ag/AgCl reference electrode and a Pt counter electrode. Figure 5 shows the voltammograms for the 20%, 25%, and 30% MXene films and their comparison. The CV curves demonstrate a progressive increase in current response and enclosed voltammetric area with increasing MXene content, indicating that the films became more electrochemically active as the conductive phase increased and more electronically connected and ion-accessible regions developed within the composite.

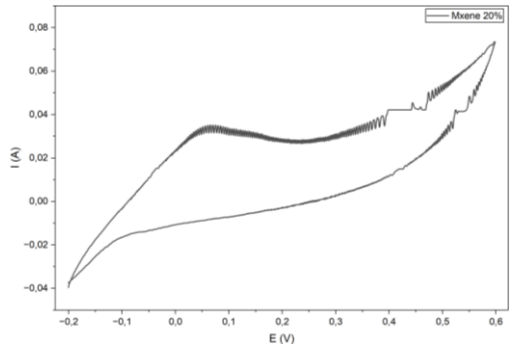

(a)

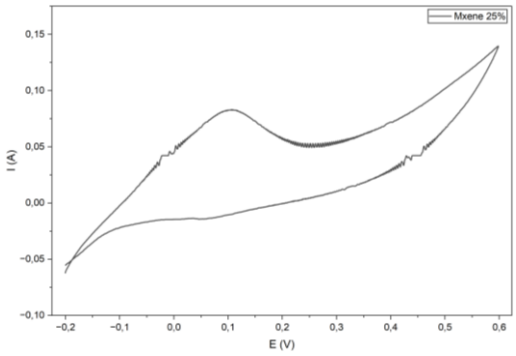

(b)

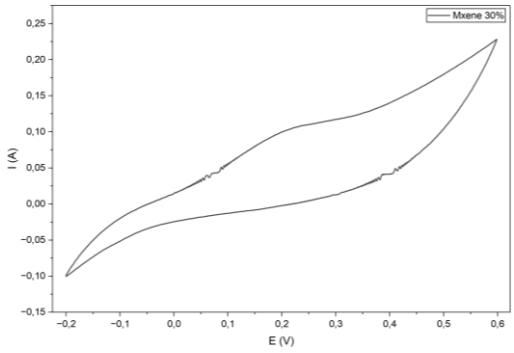

(c)

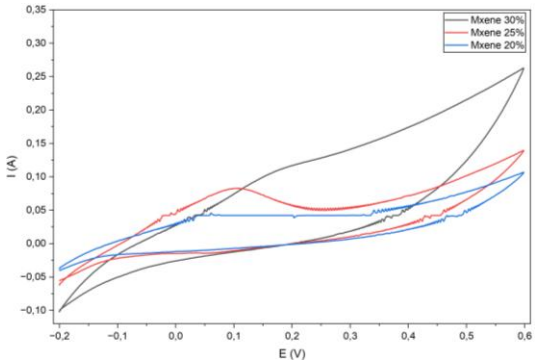

(d)

Figure 5. Voltammogram Curve for MXene loading (a)20%, (b) 25%, (c) 30% and (d) the comparison of three loadings.

The current density values derived from the CV charge current are summarized in Table 2. For the 20%, 25%, and 30% MXene films, the current densities were 425.18, 876.71, and 1480.25 A/m², respectively. These values represent increases of approximately 106.2% and 248.2% for the 25% and 30% films relative to the 20% sample, while the 30% film exceeded the 25% film by about 68.8%. This strong monotonic increase indicates that higher MXene loading improved the continuity of electron-transport pathways across the film, most likely by increasing inter-sheet connectivity and moving the composite toward a more effective percolative network. The trend is also consistent with previous findings that MXene incorporation can substantially improve electrical functionality in polymer-based composite systems [13], [14], [26]-[28].

Table 2. Current density derived from CV charge current for each MXene loading.

MXene content (%)	Electrode area (cm²)	Charge current, Ic (A)	Current density (A/cm²)	Current density (A/m²)
20	2	0.085037	0.042518	425.18
25	2	0.175342	0.087671	876.71
30	2	0.296051	0.148025	1480.25

This result is not readily comparable with current-density values reported in previous studies, because many related works focus on electrical conductivity, areal capacitance, or device-level performance rather than CV-derived current density measured under comparable alkaline electrolyte conditions [13], [14], [26]-[28]. Nevertheless, the present results are significant because they provide a controlled electrochemical comparison across a series of biodegradable PVA/ZnO/MXene/CNC films under identical preparation and testing conditions. When interpreted in conjunction with the FESEM observations, the current-density enhancement can be attributed to a more homogeneous filler distribution and improved conductive-network continuity at higher MXene loading, which together are expected to reduce transport interruptions and facilitate charge transfer across the film.

Specific Capacitance and Structure-Performance Correlation

The specific capacitance values calculated from the CV response at a scan rate of 5 mV/s are presented in Table 3. The specific

capacitance increased from 0.921966 F/g for the 20% MXene film to 1.682536 F/g for the 25% film and 2.860035 F/g for the 30% film. Relative to the 20% sample, these values correspond to capacitance increases of approximately 82.5% and 210.2% for the 25% and 30% films, respectively, while the 30% film showed a further 69.9% increase over the 25% film. These results indicate that increasing MXene loading not only improved charge transport but also enhanced the effective utilization of electroactive surfaces, likely because better filler distribution increased the fraction of MXene domains that remained accessible to electrolyte ions during CV measurement.

Table 3. Specific capacitance derived from CV for each MXene loading (scan rate 5 mV/s, mass 0.028 g).

MXene content (%)	Scan rate (mV/s)	Mass (g)	Charge current (A)	Discharge current (A)	Specific capacitance (F/g)
20	5	0.028	0.085037	−0.044037	0.921966
25	5	0.028	0.175342	−0.060212	1.682536
30	5	0.028	0.296051	−0.104353	2.860035

This capacitance trend is consistent with the known charge-storage characteristics of MXene-based systems, in which higher accessible MXene content can improve both electrical double-layer behavior and pseudocapacitive contribution, provided that the filler remains sufficiently dispersed and electrochemically accessible [25]-[28]. In the present study, FESEM observations suggest that electrochemical accessibility progressively improved from 20% to 30% MXene, which may explain why capacitance increased in parallel with morphological uniformity, as a more uniform structure would be expected to expose a larger active interfacial area and support more efficient ion transport.

The specific capacitance values obtained in this study remain lower than those reported for highly optimized MXene electrodes or fully assembled supercapacitor devices, such as pure or modified MXene systems, integrated microsupercapacitors, and advanced solid-state device architectures [15], [26]-[28]**.** However, these systems differ substantially from the present biodegradable multicomponent cast-film platform in terms of composition, architecture, electrolyte configuration, and current-collector design. A more relevant comparison can therefore be made with studies of polymer/MXene composite films. For example, Tan et al. [14] reported increased electrical conductivity in PVA/MXene thin films, while Sobolčiak et al. [13] observed improved electrical properties in PVA/CNC nanofibers after the introduction of $Ti_3C_2T_x$ MXene; however, these studies evaluated different material formats and performance parameters from those considered here**.** Although those studies did not report CV-derived specific capacitance under the same conditions as in the present work, they support the same general conclusion: increasing the MXene content and properly dispersing it in a PVA-based matrix improve the functional electrochemical behavior of the resulting composite film.

The trends in current density and specific capacitance are summarized in Figures 6 and 7, respectively. Taken together, Figures 1–7 and Tables 1–3 demonstrate that increasing MXene loading from 20% to 30% resulted in higher crystallinity, a more homogeneous morphology, a higher current density, and a higher specific capacitance. These findings support a clear structure–performance relationship, in which improved filler dispersion and conductive-network formation enhance electrochemical behavior by simultaneously facilitating electron transport and increasing the accessibility of electroactive interfaces in the biodegradable PVA/ZnO/MXene/CNC composite films.

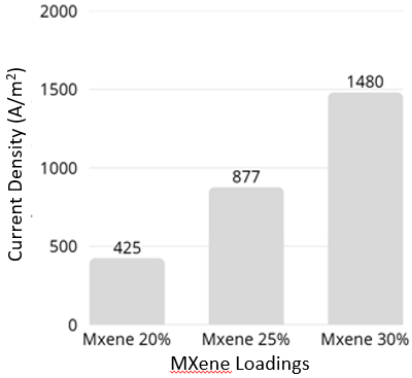

Figure 6. Current density as MXene loading increases.

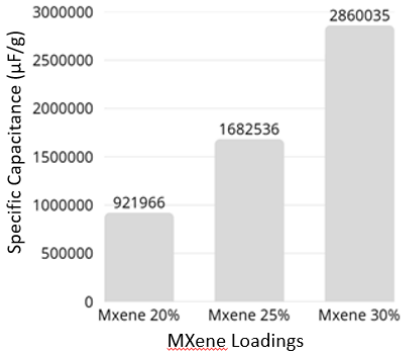

Figure 7. Specific capacitance as MXene loading increases.

Mechanistic Interpretation and Limitations

The overall results can be interpreted within a dispersion–percolation framework. At lower MXene loading, the conductive domains remain less interconnected, so charge transport is more easily interrupted and fewer electroactive regions can participate effectively, resulting in lower current density and lower specific capacitance. As the MXene content increases, the probability of forming a continuous conductive network also increases, provided that the nanosheets remain sufficiently dispersed, because shorter inter-sheet distances and more frequent filler contacts favor the establishment of percolative electron-transport pathways. In the present system, the combination of CNC-assisted spacing, controlled solution mixing, and ultrasonication appears to have produced a favorable dispersion regime in which increasing MXene loading enhanced conductive-network continuity and electroactive surface utilization without yet causing aggregation-related losses to dominate [25], [30].

At the same time, the observed monotonic trend should be interpreted within the investigated composition range only. The present data demonstrate that performance improved from 20% to 30% MXene, but they do not establish whether this trend would continue at higher loading. In MXene-based composites, excessive filler content may eventually promote restacking, reduce ion-accessible surface area, increase viscosity during

https://doi.org/10.25077/jnte.v15n1.1555.2026

casting, or compromise mechanical flexibility [25]-[30]. Moreover, the current study is based primarily on XRD, FESEM, and CV analysis. Complementary techniques such as electrochemical impedance spectroscopy, galvanostatic charge–discharge testing, long-term cycling evaluation, and mechanical characterization would be necessary to fully resolve the transport mechanism and practical performance limits of the material system.

Overall, the results and discussion demonstrate that the 30% MXene film exhibited the best performance within the investigated range, as it achieved the most favorable balance among structural ordering, morphological uniformity, and electrochemical accessibility. The present study therefore contributes a controlled loading-dependent analysis of biodegradable PVA/ZnO/MXene/CNC composite films, while maintaining clear linkage among structural, morphological, and electrochemical evidence [13], [14], [25]-[28].

CONCLUSIONS

This study demonstrated that increasing the $Ti_3C_2T_x$ MXene loading from 20% to 30% in biodegradable PVA/ZnO/MXene/CNC composite films systematically improved both structural and electrochemical properties. Among the investigated compositions, the film containing 30% MXene exhibited the highest crystallinity, the most homogeneous morphology, the highest current density, and the highest specific capacitance, indicating the most effective conductive-network formation within the tested range. The combined XRD, FESEM, and cyclic voltammetry results further suggest that the enhanced electrochemical performance was closely associated with improved filler dispersion, greater structural uniformity, and increased electroactive surface accessibility. Accordingly, the main contribution of this work is establishing a clear relationship among MXene loading, structure, and electrochemical performance in biodegradable PVA/ZnO/MXene/CNC composite films under controlled processing conditions. These findings help address the limited availability of systematic MXene-loading studies in biodegradable multicomponent film systems and provide useful insights into how the content of conductive fillers influences charge-transport continuity and capacitive behavior in sustainable flexible energy-storage materials. Nevertheless, these conclusions should be interpreted within the investigated composition range, since the superior performance of the 30% MXene film does not necessarily indicate a universal optimum, and higher loading levels may introduce restacking, transport limitations, or mechanical trade-offs. Future studies should therefore extend the MXene-loading range, include control formulations to clarify the individual roles of ZnO and CNC, and incorporate complementary electrochemical, mechanical, and biodegradation analyses to better evaluate the practical potential of this composite-film platform for sustainable flexible electronic and energy-storage applications.

ACKNOWLEDGMENT

The author would like to thank Laboratorium Material Teknik, Departemen Teknik Mesin and Laboratorium Penelitian, Departemen Teknik Lingkungan, Fakultas Teknik – Universitas Andalas

REFERENCES

[1] S. C. Teixeira, N. O. Gomes, T. V. de Oliveira, P. Fortes-Da-Silva, N. de F. F. Soares, and P. A. Raymundo-Pereira, "Review and Perspectives of sustainable, biodegradable, eco-friendly and flexible electronic devices and (Bio)sensors," *Biosensors and Bioelectronics: X*, vol. 14, 2023, doi: https://doi.org/10.1016/j.biosx.2023.100371.

[2] X. Zhuang, F. Wang, and X. Hu, "Biodegradable polymers: A promising solution for green energy devices," *European Polymer Journal*, vol. 204, p. 112696, Jan. 2024, doi: https://doi.org/10.1016/j.eurpolymj.2023.112696.

[3] R. Phiri, S. Mavinkere Rangappa, S. Siengchin, O. P. Oladijo, and T. Ozbakkaloglu, "Advances in lightweight composite structures and manufacturing technologies: A comprehensive review," *Heliyon*, vol. 10, no. 21, p. e39661, 2024, doi: https://doi.org/10.1016/j.heliyon.2024.e39661

[4] Q. Gao, S. Agarwal, A. Greiner, and T. Zhang, "Electrospun fiber-based flexible electronics: Fiber fabrication, device platform, functionality integration and applications," *Progress in Materials Science*, vol. 137, p. 101139, Aug. 2023, doi: https://doi.org/10.1016/j.pmatsci.2023.101139.

[5] B. Liu, S. Zhang, M. Li, Y. Wang, and D. Mei, "Metal–Organic Framework/Polyvinyl Alcohol Composite Films for Multiple Applications Prepared by Different Methods," *Membranes*, vol. 13, no. 9, p. 755, Aug. 2023, doi: https://doi.org/10.3390/membranes13090755.

[6] N. A. Althubiti, A. Atta, E. Abdeltwab, N. Al-Harbi, and M. M. Abdel-Hamid, "Structural characterization and dielectric properties of low energy hydrogen beam irradiated PVA/ZnO nanocomposite materials," *Inorganic Chemistry Communications*, vol. 153, p. 110779, Jul. 2023, doi: https://doi.org/10.1016/j.inoche.2023.110779.

[7] A. Wang, S. Sun, and S. Yu, "Preparation of nano zinc oxide composite porous membrane and its material regulation," *Results in Engineering*, vol. 20, 2023, doi: 10.1016/j.rineng.2023.101450.

[8] S. Asadpour, A. Raeisi vanani, M. Kooravand, and A. Asfaram, "A review on zinc oxide/poly(vinyl alcohol) nanocomposites: Synthesis, characterization and applications," Journal of Cleaner Production, vol. 362, p. 132297, Aug. 2022, doi: 10.1016/j.jclepro.2022.132297.

[9] W. R. Fadila, Abrar, and M. Nasir, "Pengaruh Heat Treatment Pada Sifat Kristal, Listrik Dan Optik Nanokomposit," *E-Proceeding Of Engineering*, vol. 9, no. 3, 2022.

[10] S. Bandaru, A. M. Jastrzębska, and M. Birowska, "Recent progress in thermoelectric MXene-based structures versus other 2D materials," *Applied Materials Today*, vol. 34, p. 101902, Oct. 2023, doi: 10.1016/j.apmt.2023.101902.

[11] C. Huang *et.al.*, "Strong and flexible MXene-based nanocomposite films for atomic oxygen resistance and electromagnetic interference shielding," *Composites Science and Technology*, vol. 253, p. 110665, 2024, doi: https://doi.org/10.1016/j.compscitech.2024.110665.

[12] B. Sindhu, V. Adepu, P. Sahatiya, and S. Nandi, "An MXene based flexible patch antenna for pressure and level sensing

applications," *FlatChem*, vol. 33, p. 100367, May 2022, doi: 10.1016/j.flatc.2022.100367.

[13] P. Sobolčiak *et al.*, "2D Ti3C2Tx (MXene)-reinforced polyvinyl alcohol (PVA) nanofibers with enhanced mechanical and electrical properties," *PLOS One*, vol. 12, no. 8, 2017, doi: 10.1371/journal.pone.0183705.

[14] K. H. Tan, L. Samylingam, N. Aslfattahi, R. Saidur, and K. Kadirgama, "Optical and conductivity studies of polyvinyl alcohol-MXene (PVA-MXene) nanocomposite thin films for electronic applications," *Optics & Laser Technology*, vol. 136, p. 106772, Apr. 2021, doi: https://doi.org/10.1016/j.optlastec.2020.106772.

[15] P. E. Lokhande *et al.*, "Etching duration as a key parameter for tailoring Ti3C2Tx MXene electrochemical properties," *Journal of Physics and Chemistry of Solids*, vol. 207, 2025, doi: https://doi.org/10.1016/j.jpcs.2025.112902.

[16] A. B. Talipova, V. V. Buranych, I. S. Savitskaya, O. V. Bondar, A. Turlybekuly, and A. D. Pogrebnjak, "Synthesis, Properties, and Applications of Nanocomposite Materials Based on Bacterial Cellulose and MXene," *Polymers*, vol. 15, no. 20, p. 4067, Oct. 2023, doi: https://doi.org/10.3390/polym15204067.

[17] B. Sun, P. Wang, Z. Liang, Z. Li, and Q. Ma, "MoS_2 /MXene Van der Waals heterojunction-based electrochemiluminescence sensor for triple negative breast cancer detection," *Talanta*, vol. 277, p. 126343, Sep. 2024, doi: https://doi.org/10.1016/j.talanta.2024.126343.

[18] J. Zhao, Z. Wang, S. Xu, H. Wang, Y. Li, and C. Fang, "Flexible bilayer Ti3C2Tx MXene/cellulose nanocrystals/waterborne polyurethane composite film with excellent mechanical properties for electromagnetic interference shielding," *Colloids and Surfaces A: Physicochemical and Engineering Aspects*, vol. 669, 2023, doi: https://doi.org/10.1016/j.colsurfa.2023.131556.

[19] R. Laghaei et al., "Reinforcement contribution of cellulose nanocrystals (CNCs) to tensile properties and fracture behavior of triaxial E-glass fabric/epoxy composites," *Composites Part A: Applied Science and Manufacturing*, vol. 164, p. 107258, Jan. 2023, doi: https://doi.org/10.1016/j.compositesa.2022.107258.

[20] A. Mohammadpour-Haratbar, Y. Zare, N. Gharib, and K. Y. Rhee, "Effect of interphase region on the Young's modulus of polymer nanocomposites reinforced with cellulose nanocrystals," *Surfaces and Interfaces*, vol. 39, 2023, doi: 10.1016/j.surfin.2023.102922.

[21] M. N. F. A. Malek *et al.*, "Ultrasonication: a process intensification tool for methyl ester synthesis: a mini review," *Biomass Conversion and Biorefinery*, vol. 13, no. 2, pp. 1457–1467, Oct. 2020, doi: https://doi.org/10.1007/s13399-020-01100-6

[22] Ł. Dybowska-Sarapuk, W. Sosnowicz, A. Grzeczkowicz, J. Krzemiński, and M. Jakubowska, "Ultrasonication effects on graphene composites in neural cell cultures," *Frontiers in Molecular Neuroscience*, vol. 15, 2022, doi: 10.3389/fnmol.2022.992494

[23] Z. Wu *et al.*, "Ultrasound-assisted preparation of chitosan/nano-silica aerogel/tea polyphenol biodegradable films: Physical and functional properties," *Ultrasonics Sonochemistry*, vol. 87, p. 106052, Jun. 2022, doi: https://doi.org/10.1016/j.ultsonch.2022.106052

[24] W. Guo *et al.*, "An efficient aeration-ultrasonic process for preparing SiCp/AZ61 composites," *Materials Science and Engineering: A*, vol. 936, p. 148425, Jul. 2025, doi: https://doi.org/10.1016/j.msea.2025.148425

[25] Y. Liu, X. Lv, Y. Song, Q. Ao, B. Yuan, T. Huanget al., "Sustainable and Tough MXene Hydrogel Based on Interlocked Structure for Multifunctional Sensing", *ACS Sustainable Chemistry & Engineering*, vol. 11, no. 10, Feb 2023. https://doi.org/10.1021/acssuschemeng.2c06939

[26] Q. Zhou, C. Zhu, H. Xue, L. Jiang, & J. Wu, "Flexible, Wearable Wireless-Charging Power System Incorporating Piezo-Ultrasonic Arrays and MXene-Based Solid-State Supercapacitors", *ACS Applied Materials & Interfaces*, vol. 16, no. 27, 2024. https://doi.org/10.1021/acsami.4c03143

[27] K. Manoharan, "Integrated health monitoring system with flexible asymmetric supercapacitors based on 2D Ti_3C_2 MXene and transitional metal oxides", NPJ Flexible Electronics, vol. 9, no. 1, Dec 2025. https://doi.org/10.1038/s41528-025-00489-2

[28] H. Xue, P. Huang, M. Göthelid, A. Strömberg, F. Niklaus, & J. Li, "Ultrahigh-Rate On-Paper PEDOT:PSS-Ti2C Microsupercapacitors with Large Areal Capacitance", *Advanced Functional Materials*, vol. 34, no. 49, 2024. https://doi.org/10.1002/adfm.202409210

[29] X. Di, Y. Zhang, H. Yu, L. Li, G. Wang, R. Zhanget al., "An ultra-stretchable, highly resilient, and degradable dual physically crosslinked hydrogel for multifunctional sensing and self-powered human–machine interaction", *Journal of Materials Chemistry A*, vol. 13, no. 38, p. 32716-32730, 2025. https://doi.org/10.1039/d5ta04671h

[30] Z. Li, "Synergistic Effects of MXene and Carbon Nanotubes in Multi-Stimuli-Responsive Chitosan Materials: Combining Shape Memory and Electromagnetic Shielding Functions", *Coatings*, vol. 15, no. 11, p. 1332, 2025. https://doi.org/10.3390/coatings15111332

[31] S. S. Poongavanam, V. Subramaniyan, P. S. Sellamuthu, J. Jarugala, and E. R. Sadiku, "Fabrication of Bio-Nanocomposite Packaging Films with PVA, MMt Clay Nanoparticles, CNCs, and Essential Oils for the Postharvest Preservation of Sapota Fruits," *Polymers (Basel)*, vol. 15, no. 17, 2023, doi: 10.3390/polym15173589.

https://doi.org/10.25077/jnte.v15n1.1555.2026